Acta Pharmaceutica Sinica B 2014;4(6):430–437

HOSTED BY

ELSEVIER

Chinese Pharmaceutical Association
Institute of Materia Medica, Chinese Academy of Medical Sciences

Acta Pharmaceutica Sinica B

www.elsevier.com/locate/apsb
www.sciencedirect.com

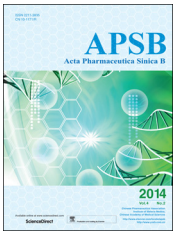

ORIGINAL ARTICLE

Inhibition of acetylcholinesterase by two genistein derivatives: kinetic analysis, molecular docking and molecular dynamics simulation

Jiansong Fang[a], Ping Wu[a], Ranyao Yang[a], Li Gao[a], Chao Li[a], Dongmei Wang[a], Song Wu[a,c], Ai-Lin Liu[a,b,c,*], Guan-Hua Du[a,b,c,*]

[a]*Institute of Materia Medica, Chinese Academy of Medical Sciences and Peking Union Medical College, Beijing 100050, China*
[b]*Beijing Key Laboratory of Drug Target Research and Drug Screening, Beijing 100050, China*
[c]*State Key Laboratory of Bioactive Substance and Function of Natural Medicines, Beijing 100050, China*

Received 13 July 2014; revised 27 August 2014; accepted 24 September 2014

KEY WORDS

Genistein derivatives;
Acetylcholinesterase (AChE);
Kinetics analysis;
Molecular docking;
Molecular dynamics simulation;
MM/GBSA

Abstract In this study two genistein derivatives (G1 and G2) are reported as inhibitors of acetylcholinesterase (AChE) and butyrylcholinesterase (BuChE), and differences in the inhibition of AChE are described. Although they differ in structure by a single methyl group, the inhibitory effect of G1 (IC_{50} = 264 nmol/L) on AChE was 80 times stronger than that of G2 (IC_{50} = 21,210 nmol/L). Enzyme-kinetic analysis, molecular docking and molecular dynamics (MD) simulations were conducted to better understand the molecular basis for this difference. The results obtained by kinetic analysis demonstrated that G1 can interact with both the catalytic active site and peripheral anionic site of AChE. The predicted binding free energies of two complexes calculated by the molecular mechanics/generalized born surface area (MM/GBSA) method were consistent with the experimental data. The analysis of the individual energy terms suggested that a difference between the net electrostatic contributions ($\Delta E_{ele}+\Delta G_{GB}$) was responsible for the binding affinities of these two inhibitors. Additionally, analysis of the molecular mechanics and MM/GBSA free energy decomposition revealed that the

Abbreviations: ACh, acetylcholine; AChEIs, acetylcholinesterase inhibitors; AChE, acetylcholinesterase; AD, Alzheimer's disease; BuChE, butyrylcholinesterase; BuSCh, *S*-butyrylthiocholine chloride; CAS, catalytic active site; DTNB, 5,5′-dithiobis-(2-nitrobenzoic acid); GAFF, generalized AMBER force field; G1, 3-(4-methoxyphenyl)-7-(2-(piperidin-1-yl)ethoxy)-4*H*-chromen-4-one; G2, (*S*)-3-(4-methoxyphenyl)-7-(2-(2-methylpiperidin-1-yl)ethoxy)-4*H*-chromen-4-one; iso-OMPA, tetraisopropyl pyrophosphoramide; MD, molecular dynamics; MM/GBSA, molecular mechanics/generalized born surface area; PAS, peripheral anionic site; PDB, protein data bank; PME, particle mesh Ewald; RMSD, root-mean-square deviation; *S*-ACh, acetylthiocholine iodide; ΔE_{ele}, electrostatic energy contribution; ΔE_{MM}, gas-phase interaction energy between receptor and ligand; ΔE_{vdw}, van der Waals energy contribution; SASA, solvent accessible surface area; ΔG_{exp}, experimental binding free energy; ΔG_{GB}, polar desolvation energy term; ΔG_{pred}, total binding free energy; ΔG_{SA}, nonpolar desolvation energy term; ΔS, conformational entropy contribution

*Corresponding authors at: Institute of Materia Medica, Chinese Academy of Medical Sciences and Peking Union Medical College, Beijing 100050, China. Tel./fax: +86 10 63165184.

E-mail addresses: liuailin@imm.ac.cn (Ai-Lin Liu), dugh@imm.ac.cn (Guan-Hua Du).

Peer review under responsibility of Institute of Materia Medica, Chinese Academy of Medical Sciences and Chinese Pharmaceutical Association.

http://dx.doi.org/10.1016/j.apsb.2014.10.002

difference between G1 and G2 originated from interactions with Tyr124, Glu292, Val294 and Phe338 of AChE. In conclusion, the results reveal significant differences at the molecular level in the mechanism of inhibition of AChE by these structurally related compounds.

1. Introduction

Alzheimer's disease (AD), a progressively degenerative disorder of the brain, is believed to be a multifactorial syndrome with several target proteins contributing to its etiology[1]. AD is characterized by a loss of basal forebrain neurons and reduced cortical and hippocampal levels of acetylcholine (ACh). The relation between the observed cholinergic dysfunction and AD severity provides a rationale for the therapeutic use of acetylcholinesterase inhibitors (AChEIs)[2].

The inhibition of acetylcholinesterase (AChE, E.C. 3.1.1.7), which is responsible for the breakdown of ACh, has been proven as a successful way to relieve some cognitive and behavioral symptoms of AD[3,4]. So far, several AChE inhibitors (Fig. 1), such as tacrine[5], galanthamine[6], huperzine A[7] and donepezil[8] have been used mainly for the clinical treatment of AD, all of which slow down neurodegeneration in AD patients to some extent.

The three-dimensional structure of AChE, as determined by X-ray crystallography for a large number of enzyme–ligand complexes[9–11], reveals two main binding sites: the catalytic active site (CAS), comprising the Ser-His-Glu catalytic triad, and the peripheral anionic site (PAS), connected by a deep, hydrophobic gorge.

Tacrine is the first AChE inhibitor permitted by the FDA. The co-crystal structure of AChE (protein data bank entry:1ACJ) from *Torpedo californica* complexed with tacrine showed that tacrine only interacted with the CAS of AChE[12]. However, due to its adverse effects such as acute liver toxicity and increased rates of syncope, tacrine has been gradually withdrawn from market. Since then, pharmaceutical chemistry scientists have become interested searching for AChE inhibitors able to simultaneously bind to their CAS and PAS. Several types of dual-binding-site AChE inhibitors have been developed by connecting the two interacting units through a suitable linker, which were generally derived from known AChE inhibitors either commercialized or under development[13–23].

To date, donepezil (PDB entry: 4EY7) is the only dual binding site AChE inhibitor approved for the treatment of AD[24]. The latest X-ray crystallographic structure of the complex between recombinant human AChE and donepezil reveals that the elongated structure of donepezil spans the entire length of the enzyme-active-site gorge[25]. It has a unique orientation along the active-site gorge, extending from the CAS, at the bottom near Trp86, to the PAS at the top near Trp286. This provides a more accurate platform for further design of next-generation derivatives.

In the current work, two genistein derivatives (G1 and G2) have been discovered with strong or moderate activity against both AChE and butyrylcholinesterase (BuChE). Although G1 and G2 (Fig. 1) have quite similar structures, experimental data in this study show that the inhibitory effect of G1 against AChE was almost 80 times greater than that of G2. Since their inhibitory mechanisms against AChE are still unclear, it is of great interest to investigate why these two analogs have differing inhibitory potencies and to reveal the molecular basis for their binding to AChE. Thus, the binding mechanisms of these two inhibitors were studied by multiple approaches consisting of enzyme-kinetic analysis, molecular docking and molecular dynamics (MD) simulation[26–41]. This study provides a molecular basis for understanding how different configurations influence their binding affinities.

2. Materials and methods

2.1. *In vitro* inhibition studies on AChE and BuChE

AChE (E.C. 3.1.1.7) was extracted from rat cortex (Sprague Dawley). BuChE (E.C. 3.1.1.8) was obtained from human plasma (purchased from Beijing Red Cross Blood Center). 5,5′-dithiobis-(2-nitrobenzoic acid) (Ellman's reagent, DTNB), acetylthiocholine iodide (*S*-ACh), *S*-butyrylthiocholine chloride (BuSCh), donepezil

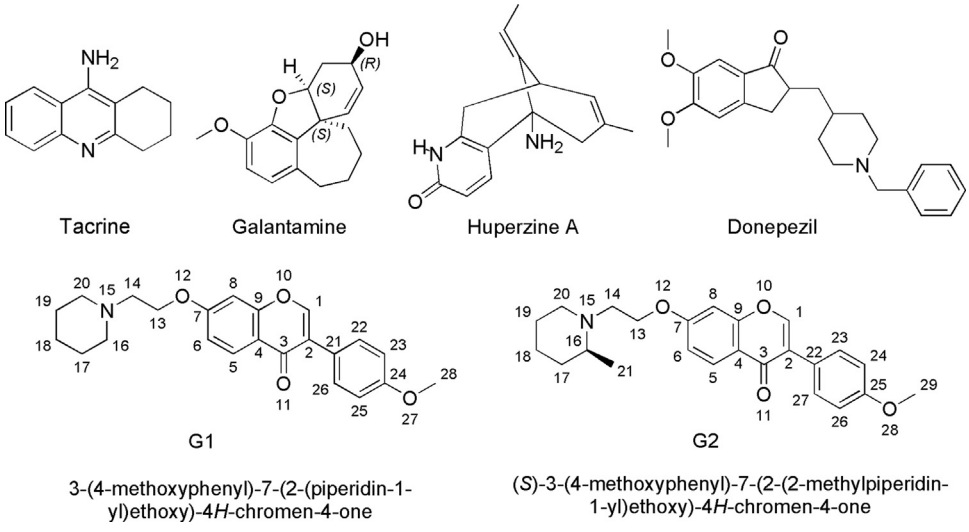

Figure 1 The structures of AChE inhibitors.

hydrochloride and tetraisopropyl pyrophosphoramide (iso-OMPA) were purchased from Sigma-Aldrich. The AChE/BuChE activity was evaluated by detecting the hydrolysis product of the substrate following the method of Ellman[42]. Five serial dilutions of G1, G2 and the reference compounds were utilized during the inhibition of AChE/BuChE activity.

In the AChE reaction system, the inhibition assay was carried out in 96-well plates using a Spectra Max M5 microplate reader (Molecular Devices, Sunnyvale, CA, USA). Donepezil hydrochloride was chosen as the reference compound. The reaction system consisted of 10 μL of test compounds, 30 μL of 0.05 mol/L PBS, 20 μL of AChE, 60 μL of 3.75 mmol/L of substrate *S*-ACh and 80 μL of 0.25 mg/mL DTNB. The assay mixture was incubated at 37 °C for 60 min and the absorbance was measured at 412 nm. Each concentration was analyzed in triplicate, and IC_{50} values were determined graphically from log concentration–inhibition curves.

In vitro BuChE assay was similar to the method described above. iso-OMPA served as the reference compound. The assay solution consisted of 10 μL of test compounds, 40 μL of BuChE, 70 μL of 7.5 mmol/L of substrate (BuSCh) and 80 μL of 0.25 mg/mL DTNB.

2.2. Kinetic characterization of AChE inhibition

The kinetic studies of G1 against AChE were performed using rat cortex homogenate as an AChE source. Enzyme activities were determined at 37 °C using five concentrations (50 μmol/L, 100 μmol/L, 200 μmol/L, 300 μmol/L and 500 μmol/L) of ACh in the presence or absence of three concentrations (110 nmol/L, 330 nmol/L and 1000 nmol/L) of G1. Kinetic characterization of the hydrolysis of Ach catalyzed by AChE was performed spectrometrically at 412 nm. The OD value was read for 50 min at 2-min intervals. Then the data were plotted on a Lineweaver–Burk diagram to reveal the mechanism of inhibition.

2.3. Molecular docking

The crystal structure of recombinant human AChE in complex with donepezil at a resolution of 2.35 Å was downloaded from the PDB (PDB entry: 4EY7), and was used as the initial 3D model. To obtain the docking–binding models for AChE in complexes with G1 and G2, the molecular modeling program MOE 2010 (Chemical Computing Group. Inc., Canada) was used to perform the docking process. At first, crystallographic water molecules were removed from 4EY7, while the active site pocket was defined by the ligand of donepezil. The detailed parameters were set as follows: the placement method, the first scoring function rescoring 1, and the saved poses were set to Triangle Matcher, London dG, and 30, respectively. In addition, the refinement, the second refinement scoring function rescoring 2, and the saved poses were set to forcefield, none, and 10, respectively.

After the docking parameters were set, the crystal pose of donepezil was first re-docked into the binding site pocket of AChE, and the root-mean-square deviation (RMSD) values between the docking and initial poses were calculated. Two systems were then prepared. System 1, named AChE/G1 complex, was AChE in complex with G1, whereas system 2, called AChE/G2, was AChE in complex with G2.

2.4. MD simulations

The AMBER 12 software was used to perform all the MD simulations in this study[43]. The inhibitors were minimized using the HF/6-31G* optimization in Gaussian 09[44], and the atom partial charges were obtained by fitting the electrostatic potentials derived by Gaussian *via* the RESP fitting technique in AMBER 12[45]. The antechamber and tleap modules were used to assign the Generalized Amber Force Field (GAFF) parameters to the two systems[46]. Ff12SB force field was assigned to the receptors[47]. The complexes were neutralized by adding 10 sodium counterions, and were surrounded by a periodic box of TIP3P water molecules extended 8 Å between the box edges and solute surface[48]. Simulations were performed using PMEMD.CUDA in AMBER 12[43]. Periodic boundary conditions were applied to avoid the edge effect. The Particle Mesh Ewald (PME) method was used to calculate long-range electrostatic interactions[49]. The hydrogen bonds were constrained using SHAKE algorithm[50]. For the non-bonded interactions, a residue-based cutoff of 10 Å was used.

The two complexes were energy-minimized to remove possible steric stress. At first, the solvent molecules and counter ions were relaxed during a 2000-step minimization. The first 1200 steps were carried out using the steepest descent algorithm, and the remaining 800 steps were performed with a conjugate gradient algorithm. In addition, the backbone atoms of each system were fixed for 3000 cycles before 8000 cycles of fully relaxed energy minimization. The system was then slowly heated from 0 to 300 K within 50 ps. After the heating process, a further 1000 ps of equilibration at 300 K was carried out to obtain a stable density. Afterward, an unconstrained production phase was initiated and continued for 10 ns in an NPT ensemble at 1 atm and 300 K. The time step used for the MD simulations was set to 2.0 fs and the trajectory files were collected every 1 ps for the subsequent analysis. All trajectory analysis was done with the Ptraj module in AMBER 12 and examined visually using the VMD software.

2.5. MM/GBSA binding-free-energy calculations

Binding free energies were calculated using the molecular mechanics generalized-born surface area (MM/GBSA) algorithms implemented in the AMBER 12. The total binding free energy can be calculated according to the equation:

$$\begin{aligned}\Delta G_{\text{bind}} &= \Delta G_{\text{gas}} + \Delta G_{\text{solv}} - T\Delta S \\ &= \Delta E_{\text{MM}} + G_{\text{GB}} + \Delta G_{\text{SA}} - T\Delta S \\ &= \Delta E_{\text{vdw}} + E_{\text{ele}} + G_{\text{GB}} + \Delta G_{\text{SA}} - T\Delta S \end{aligned} \quad (1)$$

where ΔE_{MM} denotes the gas-phase interaction energy between receptor and ligand (including van der Waals energy contribution (ΔE_{vdw}) and electrostatic energy contribution (ΔE_{ele})); ΔG_{GB} and ΔG_{SA} stand for the polar and nonpolar components of the desolvation free energy, respectively; $T\Delta S$ represents the conformational entropy contribution at temperature T. Here, ΔG_{GB} was determined by the Generalized-Born approximation model, while ΔG_{SA} was estimated based on the solvent accessible surface area (SASA) model by LCPO method: $\Delta G_{\text{SA}} = 0.0072 \times \text{SASA}$[51].

In general, due to the relatively high computational demand of calculation of entropy in AMBER 12 and the error that may introduce significant uncertainty in the results, as well as the slight variation of substitution in genistein derivatives, the conformational entropy was not considered.

Table 1 The inhibitory effect of G1, G2 and the reference compounds on AChE and BuChE activities.

Compound	IC_{50} (nmol/L)[a]		Selectivity (AChE/BuChE)
	AChE	BuChE	
G1	264 ± 24	5746 ± 144	21.8
G2	21,210 ± 4965	25,846 ± 7,040	1.2
Donepezil[54]	26 ± 6	–	–
ISO-OMPA[55]	–	2440 ± 170	–

[a]Note: Data are expressed as mean ± SD, $n = 3$.

The interaction between inhibitors and each residue was computed using the MM/GBSA decomposition procedure in AMBER 12. The binding interaction of each ligand-residue pair includes three terms: ΔE_{vdw}, ΔE_{ele}, and solvation contribution ($\Delta G_{GB} + \Delta G_{SA}$). ΔG_{GB} (the polar part) was calculated using the Generalized-Born model,[52] while ΔG_{SA} (the non-polar part) was determined with the ICOSA method.

All energy components were computed by using the same 100 snapshots extracted from 5 to 10 ns. The free energy decomposition calculation could give insight into the mechanisms of inhibition of AChE by genistein derivatives and clarify the molecular basis for their different binding affinities.

3. Results and discussion

3.1. *Inhibitory effect of G1 and G2 towards cholinesterase activities*

As given in Table 1, donepezil hydrochloride has an IC_{50} value of 26 nmol/L on AChE, which is approximately equal to that of 32 nmol/L reported in the literature[53]. G1 is a highly potent inhibitor of AChE with an IC_{50} value of 264 nmol/L, while G2 shows a moderate inhibitory effect toward AChE with an IC_{50} value of 21,210 nmol/L. Thus, the inhibitory potency of G1 is almost 80 times stronger that of G2 on AChE. To compare the selectivity of G1 and G2, an *in vitro* BuChE assay was also performed. The reference compound iso-OMPA exhibits an IC_{50} value of 2440 nmol/L with BuChE, which is comparable to that of 980 nmol/L reported in the literature[54]. The results (Table 1) suggest both G1 ($IC_{50} = 5746$ nmol/L) and G2 ($IC_{50} = 25{,}846$ nmol/L) can inhibit BuChE activity moderately, while G1 (selectivity = 21.8) possesses better selectivity than G2 (selectivity = 1.2).

3.2. *Kinetic study results*

Graphical analysis of the Lineweaver–Burk plot gives information about the binding mode. As shown in Fig. 2, the lines cross the third quadrant in the same point, and V_{max} decreases as the concentration of G1 increases. The Lineweaver–Burk plot reveals that G1 is a typically mixed AChE inhibitor which is similar to that of donepezil[55,56]. The result shows that G1 is able to interact with both CAS and PAS of AChE.

3.3. *Validation of molecular docking and molecular dynamics simulation methods*

To validate whether the docking software MOE was reliable for the AChE (PDB code: 4EY7) system, the crystal pose of donepezil

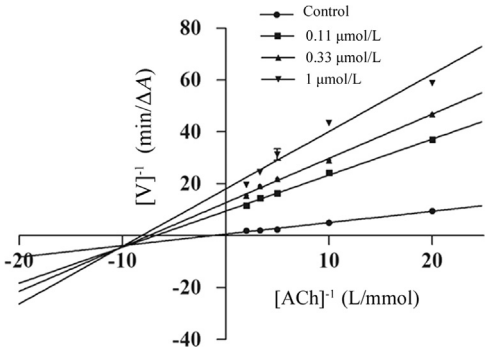

Figure 2 Steady state inhibition by G1 of AChE hydrolysis of ACh; reciprocal plots of initial velocity with substrate concentration: the plots show mixed-type inhibition for G1.

was initially re-docked into the binding site of AChE with specific docking parameters and scoring functions. The 10 generated conformations were then compared with the crystal pose. Docking was considered acceptable if the average RMSD value of the docking poses was less than a given threshold of 2.0 Å from the crystal pose. In this study, the average RMSD value of donepezil between the docking poses and the crystal conformation was 1.53 Å. This implied that MOE could reproduce the crystal-binding model and was suitable for the AChE system. Afterward, G1 and G2 were docked into the same binding site pocket of AChE by use of the same optimum docking conditions above to obtain the starting models for subsequent MD simulations.

To explore the dynamic stability of the two AChE/inhibitor complexes and to ensure the rationality of the sampling strategy, the time-dependent RMSD values of the complex backbone atoms were calculated from the X-ray crystal structure of AChE during MD trajectories of 10 ns. The RMSD plot (Fig. 3) indicates that the conformations of the AChE/G1 complex achieve equilibrium around 3200 ps and fluctuate around 1.3 Å. However, for the AChE/G2 complex, the equilibrium time is around 5000 ps and the conformations fluctuate around 1.6 Å. Both trajectories are stable after 5000 ps, so it is reasonable to do the binding free energy calculation and free energy decomposition based on the snapshots extracted from 5 to 10 ns.

For better understanding on how G1 and G2 influence the binding mode with AChE, the structural changes of two complexes were examined. To visualize the result clearly, 10 structures (snapshots) were overlaid during the MD simulations, of which coordinates were saved after every 1 ns from 1 to 10 ns. As shown in Fig. 4a, the 10 conformations of G1 undergo little movement, which means that G1 is stable throughout the MD simulation. On the other hand, in Fig. 4b, the 10 conformations of G2 undergo a large amount of movement during

the MD simulations. Therefore, this analysis suggests that AChE/G1 complex is more stable than AChE/G2 complex.

3.4. *Binding free energies calculation*

In MM/GBSA calculations, the affinity of one inhibitor binding to the receptor could be estimated using the snapshots from a trajectory of the complex. The ΔG_{exp} was estimated by the equation $\Delta G_{exp} \approx RT \ln(IC_{50})$. These values, with the values of absolute binding free energies of G1 and G2, obtained using the MM/GBSA technique, are given in Table 2. The descending trend in ΔG_{pred} for AChE/G2 and AChE/G1 complexes is consistent with that in ΔG_{exp}.

To get a better view of which energy term has more impact on the binding affinity, the four individual energy components (ΔE_{vdw}, ΔE_{ele}, ΔG_{GB} and ΔG_{SA}) were carefully compared. From Table 2, it is evident that the ΔE_{vdw} is dominant in ΔG_{pred}. The ΔE_{vdw} of AChE/G1 (−54.8 kcal/mol) complex is equal to AChE/G2 (−54.8 kcal/mol). Obviously, the ΔE_{vdw} part cannot account for the activity difference between G1 and G2. However, the ΔE_{ele} of AChE/G1 complex (−11.6 kcal/mol) is stronger than that of AChE/G2 (−3.9 kcal/mol). Considering the negative effect generated by ΔG_{GB}, the net electrostatic contributions ($\Delta E_{ele}+\Delta G_{GB}$) of AChE/G1 and AChE/G2 complexes are 17.5 and 22.1 kcal/mol, respectively, which is unfavorable for binding in the two complexes. Furthermore, the difference in the net electrostatic contribution ($\Delta E_{ele}+\Delta G_{GB}$) between G1 and G2 is −4.6 kcal/mol. In addition, both of ΔG_{SA} for the two complexes (−6.6 kcal/mol and −6.2 kcal/mol) are approximately equivalent. Therefore, the net electrostatic contributions ($\Delta E_{ele}+\Delta G_{GB}$) play the most important role in differentiating the activity between G1 and G2.

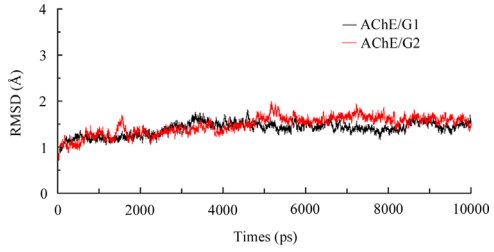

Figure 3 Root-mean-square deviation (RMSD) of the backbone atoms (CA, N, C) of the AChE/G1 and AChE/G2 complexes.

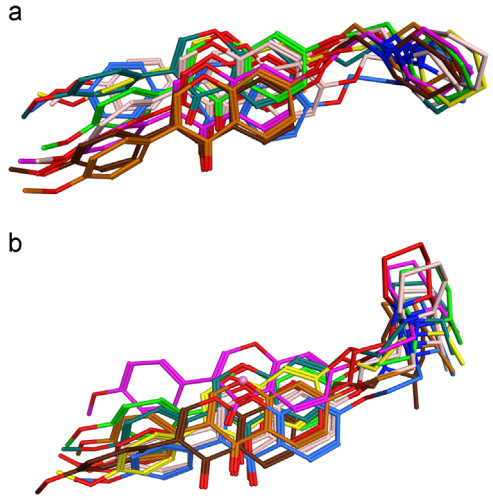

Figure 4 The superposition of 10 snapshots from 1 to 10 ns for AChE/G1 complex (a) and AChE/G2 complex (b).

3.5. *Residue-based-energy decomposition using the MM/GBSA method*

To further delineate the detailed mechanism of the AChE/inhibitor interactions, residue-based-energy decomposition was performed to evaluate the effects of energy on the contributions of each residue in the binding site pocket by using the MM/GBSA method. Fig. 5 shows the energy decomposition values for key residues in the two complexes.

Generally, if the interaction energy between a residue and a ligand is lower than −0.8 kcal/mol, the residue is regarded as an important residue in the molecular recognition of that ligand. In the AChE/G1 complex, the major favorable energy contributions (−3.02 to −0.94 kcal/mol) originate predominately from Tyr124 (−3.02), Trp341 (−2.18), Trp286 (−2.08), Glu292 (−1.49), Val294 (−1.28), Phe338 (−1.04) and Tyr72 (−0.94). In the AChE/G2 complex, the residues which give the most negative binding free energies (kcal/mol) are Trp286 (−2.79), Tyr341 (−2.43), Thr83 (−1.23), Gln291 (−0.93), Trp86 (−0.92), Tyr124 (−0.90) and Glu292 (−0.88). As shown in Fig. 5, the two inhibitors have similar interaction patterns, which means strong or moderate interactions with residue Tyr124, Trp286, Glu292 and Try341. Comparison between G1 and G2 shows that the interactions of G1 with Tyr124, Glu292, Val294 and Phe338 (−3.02, −1.49, −1.28 and −1.04 kcal/mol) are stronger than those of G2 (−0.90, −0.88, −0.20 and −0.36 kcal/mol). Therefore, it is conceivable that the difference between the inhibitory effect of G1 and G2 originates from these key residues (Tyr124, Glu292, Val294 and Phe338).

Since ΔE_{vdw} is dominant in the total binding free energy (ΔG_{pred}), it is of interest to determine if van der Waals interactions determine the different biological activities between G1 and G2. As shown in Supplementary Fig. 1, the differences in the van der Waals interactions between G1 and G2 were reported for the amino acids Trp286, Val294, Phe338 and Tyr341. The van der Waals interactions of G1 with Val294 and Phe338 (−0.97 and −1.93 kcal/mol) are stronger than those of G2 (−0.09 and −0.64 kcal/mol). However, the interactions of G1 with Trp286 and Tyr341 are weaker (−3.48 and −2.81 kcal/mol) than those of G2 (−4.28 and −3.68 kcal/mol),

Table 2 The components of the binding free energy (kcal/mol) for the AChE complexes with G1 or G2, determined by using the MM/GBSA method.

Inhibitor	ΔE_{vdw}	ΔE_{ele}	ΔG_{GB}	ΔG_{SA}	ΔG_{pred}	ΔG_{exp}
G1	−54.8±2.8	−11.6±2.2	29.1±2.2	−6.6±0.2	−43.9±2.9	−9.0
G2	−54.8±2.4	−3.9±3.2	26.0±2.8	−6.2±0.2	−38.9±2.6	−6.4

which compensates for the differences made by van der Waals interactions.

As presented in Supplementary Fig. 2, electrostatic interactions (ΔE_{ele}) between the inhibitors and the important residues were investigated to explain the different inhibitory activities between G1 and G2. It is obvious that the ΔE_{ele} of G1 with Tyr124, Glu292, Phe338 and Tyr341 (−1.97, 0.06, −0.21 and −0.44 kcal/mol) is much stronger than those of G2 (−0.94, 0.66, 0.39 and 0.33 kcal/mol). Therefore, the differences obtained from electrostatic interactions can explain the significant difference between G1 and G2.

As shown in Supplementary Fig. 3, the polar contributions of desolvation (ΔG_{GB}) were also determined. The interaction is almost opposite to the electrostatic interaction. On the whole, the net electrostatic interaction ($\Delta E_{ele}+\Delta G_{GB}$) opposes binding, which is consistent with the discussion in the section on binding free energies calculation.

3.6. *Binding mode of the AChE/G1 and AChE/G2 complexes*

Results above proposed an explanation as to why G1 was more active than G2 in terms of free energy. In fact, the energy was decided by the structure. Therefore, we analyzed whether slight structural modifications on G1 could influence the binding and eventually change the interaction with AChE. Here the average structure was based on the 100 snapshots (from 5 to 10 ns) obtained, and the binding modes in the active site pocket of AChE with G1 and G2 are displayed in Fig. 6.

As shown in Fig. 6a, G1 extends deeply into the two main binding sites of AChE. The CAS and PAS are connected by a deep, hydrophobic gorge. The piperidine ring of G1 enables hydrophobic/van der Waals interactions with Trp86 and Phe338 in the CAS, while the flavone ring of G1 stacks against Trp286 and Tyr341 in the PAS; thus G1 is sandwiched between the rings of Trp286 and Tyr341. Meanwhile, the oxygen atom at C7 in flavone ring can form a strong hydrogen bond of 2.8 Å with the –OH of Tyr124, which is consistent with decomposition analysis of the electrostatic interaction. Moreover, G1 can also make hydrophobic/van der Waals interactions with Tyr72, Glu292 and Val294.

As shown in Fig. 6b, G2 has a similar binding pattern to G1 except for some key differences. The flavone ring of G2 can also stack against Trp286 and Tyr341 in the PAS and make a hydrophobic/van der Waals interaction with Trp86 in the CAS. Because of the long distance (3.5 Å) between the oxygen atom at C7 and the –OH of Tyr124, they could not form a hydrogen-bonding interaction. In order to clearly observe the differences between the two binding modes, the two complexes were superimposed. As presented in Fig. 7, compared with G1, the methyl group substitution at C16 induces a large movement of the piperidine ring of G2 as demonstrated by MD. Therefore, some hydrophobic/van der Waals interactions (such as Tyr72, Val294 and Phe338) have disappeared.

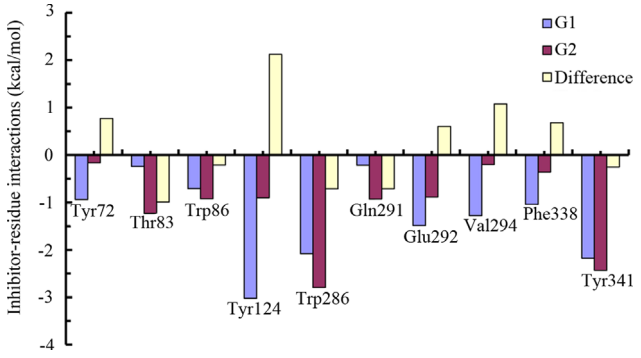

Figure 5 The inhibitor–residue interaction spectrum for AChE/G1 and AChE/G2 complexes.

4. Conclusions

Two genistein derivatives (G1 and G2) have been discovered as inhibitors of AChE and BuChE in this investigation. The absence (G1) or presence (G2) of a methyl group resulted in a distinct difference in their inhibitory activity toward AChE. The present study provided insights into the two inhibitor-bound structures of AChE. We analyzed the binding mechanisms of both inhibitors to AChE using multiple approaches including enzyme-kinetics analysis, molecular docking and MD simulation.

The results obtained by the kinetic study revealed that G1 was able to interact with both the CAS and PAS of AChE. MM/GBSA calculations predicted binding free energies of −43.9 kcal/mol (G1) and −38.9 kcal/mol (G2), which were consistent with our experimental results. It was observed that ΔE_{ele}, ΔE_{vdw} and ΔG_{SA} were the main driving forces for inhibitor binding, whereas the net electrostatic contribution ($\Delta E_{ele}+\Delta G_{GB}$) difference was the leading reason for distinguishing the binding affinities of these two inhibitors.

The structure analysis revealed that the flavone rings of the two inhibitors could stack against Trp286 and Tyr341 in the PAS, and their piperidine rings could enable hydrophobic/van der Waals interaction with Trp86 in the CAS. This may explain why

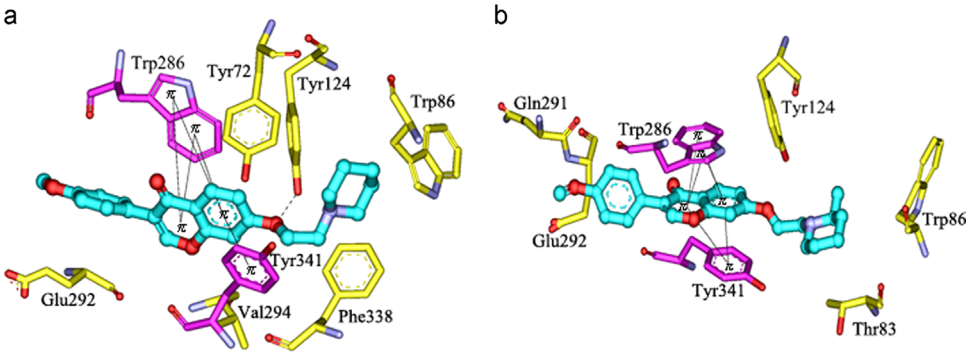

Figure 6 The binding modes of AChE/G1 (a) and AChE/G2 (b) complexes.

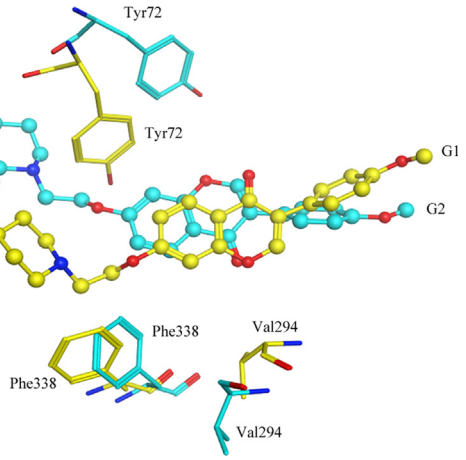

Figure 7 The superposition of AChE/G1 (yellow) complex over AChE/G2 (cyan) counterparts. (For interpretation of the references to color in this figure legend, the reader is referred to the web version of this article.)

genistein derivatives with a piperidine ring exhibit inhibition of AChE. In the binding mode of G1, van der Waals and electrostatic/H-bond interactions are the driving forces for AChE recognition. Unlike G1, the oxygen atom at C7 in G2 could not form a hydrogen bond with the –OH of Tyr124, and some hydrophobic/van der Waals' interactions (such as Tyr72, Glu292, Val294 and Phe338) had disappeared, making the inhibitory potency of G1 80 times higher than that of G2.

In summary, all the results indicated that enzyme-kinetic analysis, molecular docking and MD simulation could provide an alternative way to reveal the molecular mechanism of inhibition of AChE by genistein derivatives, and thus contribute to a better understanding of the therapeutic potential of the two inhibitors.

Acknowledgments

This work was funded in part of the Research Special Fund for Public Welfare Industry of Health (No. 200802041), the National Great Science and Technology Projects (2012ZX09301002, 2014ZX09507003-002), the International Collaboration Project (2011DFR31240), and Institue of Chinese Materia Medica, China Academy of Chinese Medical Sciences & Peking Union Medical College graduate student innovation fund (2013-1007-18). We thank Professor Jun Xu's group for providing the High Performance Supercomputer resource at Sun Yat-Sen University.

Appendix A. Supporting information

Supplementary data associated with this article can be found in the online version at http://dx.doi.org/10.1016/j.apsb.2014.10.002.

References

1. Melnikova I. Therapies for Alzheimer's disease. *Nat Rev Drug Discov* 2007;**6**:341–2.
2. Hitzeman N. Cholinesterase inhibitors for Alzheimer's disease. *Am Fam Physician* 2006;**74**:747–9.
3. Sabbagh MN. Drug development for Alzheimer's disease: where are we now and where are we headed? *Am J Geriatr Pharmacother* 2009;**7**:167–85.
4. Citron M. Alzheimer's disease: strategies for disease modification. *Nat Rev Drug Discov* 2010;**9**:387–98.
5. Davis KL, Thal LJ, Gamzu ER, Davis CS, Woolson RF, Gracon SI, et al. A double-blind, placebo-controlled multicenter study of tacrine for Alzheimer's disease. The Tacrine Collaborative Study Group. *New Engl J Med* 1992;**327**:1253–9.
6. Thomsen T, Kewitz H. Selective inhibition of human acetylcholinesterase by galanthamine *in vitro* and *in vivo*. *Life Sci* 1990;**46**:1553–8.
7. Xu SS, Gao ZX, Weng Z, Du ZM, Xu WA, Yang JS, et al. Efficacy of tablet huperzine-A on memory, cognition, and behavior in Alzheimer's disease. *Acta Pharmacol Sin* 1995;**16**:391–5.
8. AD2000 Collaborative Group. Long-term donepezil treatment in 565 patients with Alzheimer's disease (AD2000): randomised double-blind trial. *Lancet* 2004;**363**:2105–15.
9. Sussman JL, Harel M, Frolow F, Oefner C, Goldman A, Toker L, et al. Atomic structure of acetylcholinesterase from Torpedo californica: a prototypic acetylcholine-binding protein. *Science* 1991;**253**:872–9.
10. Bourne Y, Grassi J, Bougis PE, Marchot P. Conformational flexibility of the acetylcholinesterase tetramer suggested by x-ray crystallography. *J Biol Chem* 1999;**274**:30370–6.
11. Kryger G, Harel M, Giles K, Toker L, Velan B, Lazar A, et al. Structures of recombinant native and E202Q mutant human acetylcholinesterase complexed with the snake-venom toxin fasciculin-II. *Acta Crystallogr D: Biol Crystallogr* 2000;**56**:1385–94.
12. Harel M, Schalk I, Ehret-Sabatier L, Bouet F, Goeldner M, Hirth C, et al. Quaternary ligand binding to aromatic residues in the active-site gorge of acetylcholinesterase. *Proc Natl Acad Sci USA* 1993;**90**:9031–5.
13. Carlier PR, Chow ES, Han YF, Liu J, El Yazal J, Pang YP. Heterodimeric tacrine-based acetylcholinesterase inhibitors: investigating ligand-peripheral site interactions. *J Med Chem* 1999;**42**:4225–31.
14. Carlier PR, Du DM, Han YF, Liu J, Pang YP. Potent, easily synthesized huperzine A–tacrine hybrid acetylcholinesterase inhibitors. *Bioorg Med Chem Lett* 1999;**9**:2335–8.
15. Carlier PR, Han YF, Chow ES, Li CP, Wang H, Lieu TX, et al. Evaluation of short-tether bis-THA AChE inhibitors. A further test of the dual binding site hypothesis. *Bioorg Med Chem* 1999;**7**:351–7.
16. Savini L, Campiani G, Gaeta A, Pellerano C, Fattorusso C, Chiasserini L, et al. Novel and potent tacrine-related hetero- and homobivalent ligands for acetylcholinesterase and butyrylcholinesterase. *Bioorg Med Chem Lett* 2001;**11**:1779–82.
17. Alonso D, Dorronsoro I, Rubio L, Muñoz P, García-Palomero E, Del Monte M, et al. Donepezil–tacrine hybrid related derivatives as new dual binding site inhibitors of AChE. *Bioorg Med Chem* 2005;**13**:6588–97.
18. Camps P, Formosa X, Galdeano C, Muñoz-Torrero D, Ramírez L, Gómez E, et al. Pyrano[3,2-*c*]quinoline-6-chlorotacrine hybrids as a novel family of acetylcholinesterase- and beta-amyloid-directed anti-Alzheimer compounds. *J Med Chem* 2009;**52**:5365–79.
19. Zhu YP, Xiao K, Ma LP, Xiong B, Fu Y, Yu HP, et al. Design, synthesis and biological evaluation of novel dual inhibitors of acetylcholinesterase and *β*-secretase. *Bioorg Med Chem* 2009;**17**:1600–13.
20. Huang WH, Tang L, Shi Y, Huang SF, Xu L, Sheng R, et al. Searching for the multi-target-directed ligands against Alzheimer's disease: discovery of quinoxaline-based hybrid compounds with AChE, H3R and BACE 1 inhibitory activities. *Bioorg Med Chem* 2011;**19**:7158–67.
21. Peng DY, Sun Q, Zhu XL, Lin HY, Chen Q, Yu NX, et al. Design, synthesis, and bioevaluation of benzamides: novel acetylcholinesterase inhibitors with multi-functions on butylcholinesterase, A*β* aggregation, and *β*-secretase. *Bioorg Med Chem* 2012;**20**:6739–50.
22. Catto M, Pisani L, Leonetti F, Nicolotti O, Pesce P, Stefanachi A, et al. Design, synthesis and biological evaluation of coumarin alkylamines as potent and selective dual binding site inhibitors of acetylcholinesterase. *Bioorg Med Chem* 2013;**21**:146–52.
23. Camps P, Formosa X, Galdeano C, Gómez T, Muñoz-Torrero D, Scarpellini M, et al. Novel donepezil-based inhibitors of acetyl- and

butyrylcholinesterase and acetylcholinesterase-induced beta-amyloid aggregation. *J Med Chem* 2008;**51**:3588–98.
24. Sugimoto H, Iimura Y, Yamanishi Y, Yamatsu K. Synthesis and structure-activity relationships of acetylcholinesterase inhibitors: 1-benzyl-4-[(5,6-dimethoxy-1-oxoindan-2-yl)methyl]piperidine hydrochloride and related compounds. *J Med Chem* 1995;**38**:4821–9.
25. Cheung J, Rudolph MJ, Burshteyn F, Cassidy MS, Gary EN, Love J, et al. Structures of human acetylcholinesterase in complex with pharmacologically important ligands. *J Med Chem* 2012;**55**:10282–6.
26. Yu ZH, Wen X, Xi Z. Insight into herbicide resistance of W574L mutant *Arabidopsis thaliana* acetohydroxyacid synthase: molecular dynamics simulations and binding free energy calculations. *Sci China Chem* 2010;**53**:91–102.
27. Bharatham K, Bharatham N, Kwon YJ, Lee KW. Molecular dynamics simulation study of PTP1B with allosteric inhibitor and its application in receptor based pharmacophore modeling. *J Comput Aid Mol Des* 2008;**22**:925–33.
28. Chen Q, Cui W, Ji MJ. Studies of chirality effect of 4-(phenylamino)-pyrrolo[2,1-f][1,2,4]triazine on p38alpha by molecular dynamics simulations and free energy calculations. *J Comput Aid Mol Des* 2009;**23**:737–45.
29. Cheng YH, Cui W, Chen Q, Tung CH, Ji MJ, Zhang FS. The molecular mechanism studies of chirality effect of PHA-739358 on Aurora kinase A by molecular dynamics simulation and free energy calculations. *J Comput Aid Mol Des* 2011;**25**:171–80.
30. Negri M, Recanatini M, Hartmann RW. Computational investigation of the binding mode of bis(hydroxylphenyl)arenes in 17β-HSD1: molecular dynamics simulations, MM-PBSA free energy calculations, and molecular electrostatic potential maps. *J Comput Aid Mol Des* 2011;**25**:795–811.
31. Liu M, Yuan MG, Luo MX, Bu XZ, Luo HB, Hu XP. Binding of curcumin with glyoxalase I: molecular docking, molecular dynamics simulations, and kinetics analysis. *Biophys Chem* 2010;**147**:28–34.
32. Shao YX, Zhao P, Li Z, Liu M, Liu PQ, Huang M, et al. The molecular basis for the inhibition of human cytochrome P450 1A2 by oroxylin and wogonin. *Eur Biophys J* 2012;**41**:297–306.
33. Zhao P, Chen SK, Cai YH, Lu X, Li Z, Cheng YK, et al. The molecular basis for the inhibition of phosphodiesterase-4D by three natural resveratrol analogs. Isolation, molecular docking, molecular dynamics simulations, binding free energy, and bioassay. *Biochim Biophys Acta* 2013;**1834**:2089–96.
34. Huang YY, Li Z, Cai YH, Feng LJ, Wu YN, Li XS, et al. The molecular basis for the selectivity of tadalafil toward phosphodiesterase 5 and 6: a modeling study. *J Chem Inf Model* 2013;**53**:3044–53.
35. De Luca L, Morreale F, Chimirri A. Insight into the fundamental interactions between LEDGF binding site inhibitors and integrase combining docking and molecular dynamics simulations. *J Chem Inf Model* 2012;**52**:3245–54.
36. Sgobba M, Caporuscio F, Anighoro A, Portioli C, Rastelli G. Application of a post-docking procedure based on MM-PBSA and MM-GBSA on single and multiple protein conformations. *Eur J Med Chem* 2012;**58**:431–40.
37. Chang HW, Chung FS, Yang CN. Molecular modeling of p38alpha mitogen-activated protein kinase inhibitors through 3D-QSAR and molecular dynamics simulations. *J Chem Inf Model* 2013;**53**:1775–86.
38. González-Mendióroz M, Álvarez-Vázquez AB, Rubio-Martinez J. Structural analysis of the inhibition of APRIL by TACI and BCMA through molecular dynamics simulations. *J Mol Graph Model* 2013;**39**:13–22.
39. Greenidge PA, Kramer C, Mozziconacci JC, Wolf RM. MM/GBSA binding energy prediction on the PDBbind data set: successes, failures, and directions for further improvement. *J Chem Inf Model* 2013;**53**:201–9.
40. Tripathi SK, Muttineni R, Singh SK. Extra precision docking, free energy calculation and molecular dynamics simulation studies of CDK2 inhibitors. *J Theor Biol* 2013;**334**:87–100.
41. Xu L, Sun HY, Li YY, Wang J, Hou T. Assessing the performance of MM/PBSA and MM/GBSA methods. 3. The impact of force fields and ligand charge models. *J Phys Chem B* 2013;**117**:8408–21.
42. Ellman GL, Courtney KD, Andres Jr V, Featherstone RM. A new and rapid colorimetric determination of acetylcholinesterase activity. *Biochem Pharmacol* 1961;**7**:91–5.
43. Case DA, Cheatham TE, Darden T, Gohlke H, Luo R, Merz KM, et al. The Amber biomolecular simulation programs. *J Comput Chem* 2005;**26**:1668–88.
44. Frisch MJ, Trucks GW, Schlegel HB, Scuseria GE, Robb MA, Cheeseman JR, et al. *Petersson Ge Gaussian 09*. Wallingford, CT: Gaussian, Inc.; 2009. Available from: ⟨http://www.surfchem.fudan.edu.cn/teacher/lizh/Usefull_Files/g09/g_tech/g_ur/m_citation.htm⟩.
45. Bayly CI, Cieplak P, Cornell W, Kollman PA. A well-behaved electrostatic potential based method using charge restraints for deriving atomic charges: the RESP model. *J Phys Chem* 1993;**97**:10269–80.
46. Wang J, Wolf RM, Caldwell JW, Kollman PA, Case DA. Development and testing of a general amber force field. *J Comput Chem* 2004;**25**:1157–74.
47. Yang LJ, Tan C-h, Hsieh M-J, Wang JM, Duan Y, Cieplak P, et al. New-generation amber united-atom force field. *J Phys Chem B* 2006;**110**:13166–76.
48. Jorgensen WL, Chandrasekhar J, Madura JD, Impey RW, Klein ML. Comparison of simple potential functions for simulating liquid water. *J Chem Phys* 1983;**79**:926–35.
49. Darden T, York D, Pedersen L. Particle mesh Ewald: an $N\log(N)$ method for Ewald sums in large systems. *J Chem Phys* 1993;**98**:10089–92.
50. Ryckaert J-P, Ciccotti G, Berendsen HJC. Numerical integration of the cartesian equations of motion of a system with constraints: molecular dynamics of n-alkanes. *J Comput Phys* 1977;**23**:327–41.
51. Weiser J, Shenkin PS, Still WC. Approximate atomic surfaces from linear combinations of pairwise overlaps (LCPO). *J Comput Chem* 1999;**20**:217–30.
52. Onufriev A, Bashford D, Case DA. Exploring protein native states and large-scale conformational changes with a modified generalized born model. *Proteins* 2004;**55**:383–94.
53. Hu YQ, Zhang J, Chandrashankra O, Ip FCF, Ip NY. Design, synthesis and evaluation of novel heterodimers of donepezil and huperzine fragments as acetylcholinesterase inhibitors. *Bioorg Med Chem* 2013;**21**:676–83.
54. Luo WM, Yu QS, Kulkarni SS, Parrish DA, Holloway HW, Tweedie D, et al. Inhibition of human acetyl- and butyrylcholinesterase by novel carbamates of (−)- and (+)-tetrahydrofurobenzofuran and methanobenzodioxepine. *J Med Chem* 2006;**49**:2174–85.
55. Huang L, Shi A, He F, Li XS. Synthesis, biological evaluation, and molecular modeling of berberine derivatives as potent acetylcholinesterase inhibitors. *Bioorg Med Chem* 2010;**18**:1244–51.
56. Shi DH, Huang W, Li C, Wang LT, Wang SF. Synthesis, biological evaluation and molecular modeling of aloe-emodin derivatives as new acetylcholinesterase inhibitors. *Bioorg Med Chem* 2013;**21**:1064–73.